Supporting information

NiFe-nanoparticles supported N-doped graphene hollow spheres entangled with self-grown N-doped carbon nanotubes for liquid electrolyte/flexible all-solid-state rechargeable zinc-air batteries

Yefei Ma,[a,b,+] Weiheng Chen,[c,+] Zhongqing Jiang, [*a] Xiaoning Tian, [*b] Xinyi WangGuo,[b] Guangliang Chen [d] and Zhong-Jie Jiang [*e]

[a] Key Laboratory of Optical Field Manipulation of Zhejiang Province, Department of Physics, Zhejiang Sci-Tech University, Hangzhou 310018, P.R. China. E-mail: zhongqingjiang@hotmail.com or zhongqingjiang@zstu.edu.cn

[b] Department of Materials and Chemical Engineering, Ningbo University of Technology, Ningbo 315211, P.R. China. E-mail: boxertxn@hotmail.com

[c] Vehicle Energy and Safety Laboratory, Department of Mechanical Engineering, Ningbo University of Technology, Ningbo 315336, P.R. China.

[d] School of Materials Science and Engineering, Zhejiang Sci-Tech University, Hangzhou 310018, P.R. China.

[e] Guangdong Engineering and Technology Research Center for Surface Chemistry of Energy Materials & Guangzhou Key Laboratory for Surface Chemistry of Energy Materials, New Energy Research Institute, College of Environment and Energy, South China University of Technology, Guangzhou 510006, P.R. China. Email: eszjiang@scut.edu.cn or zhongjiejiang1978@hotmail.com

[+]These authors contributed equally.

This PDF file includes:

Experimental Section

Fig. S1 to S13

Tables S1-S7

1. Experimental section

1.1. Reagents and materials

Flake graphite (325 meshes) was bought from Alfa Ltd. Concentrated sulfuric acid (H_2SO_4, 96.0%), sodium nitrate ($NaNO_3$, ≥99.0%), hydrochloric acid (HCl, 37.0%), potassium hydroxide (KOH, ≥85.0%), potassium permanganate ($KMnO_4$, ≥99.5%), hydrogen peroxide aqueous solution (H_2O_2, 30.0%), 2,2'-Azobis (2-methylpropionamidine)dihydrochloride (97.0%), polyvinyl pyrrolidone (K-30), styrene (C_8H_8, ≥99.5%), melamine ($C_3H_6N_6$, ≥99.0%), 2-methylimidazole ($C_4H_6N_2$, 98％), nickel(II) nitrate hexahydrate ($Ni(NO_3)_2·6H_2O$), ≥98.0%), iron(III) nitrate nonahydrate ($Fe(NO_3)_3·9H_2O$, ≥98.5%), zinc acetate ($Zn(Ac)_2$, ≥99.0%), polyvinyl alcohol (PVA, 99.0%), and isopropanol ($CH_3CH(OH)CH_3$, ≥99.7%) were bought from Shanghai Chemical Reagent Co. Ltd. Carbon paper (CP), Carbon cloth, commercial 20% Pt/C were purchased from Shanghai Hesen Electric Co., Ltd. (Shanghai, China). RuO_2 (99.9%) and Zinc foil (99.994%) was purchased from Alfa Aesar. Nafion (5.0 wt.%) was purchased from DuPont Company. All the chemicals were used as received without further purification.

1.2. Preparation of polystyrene spheres (PS)

The positively charged polystyrene spheres (PS) were prepared by the emulsifier-free polymerization method described previously.[1] 13.0 mL styrene monomer and 1.5 g polyvinyl pyrrolidone (PVP) were dissolved in 100 mL of deionized (DI) water. The mixture was stirred for 30 min at room temperature under the protection of nitrogen. Then, 0.26 g 2,2'-Azobis (2-methylpropionamidine) dihydrochloride (AIBA) solution was added to the above-mentioned mixture under stirring and the protection of nitrogen for 1 h, which was dissolved in 20 mL DI water. Then, the reaction temperature was raised to 70 °C, and the reaction was kept under N_2 protection condition for 24 h.

1.3. Materials characterizations

The morphologies of obtained samples were characterized using field emission scanning electron microscopy (S-4800, Hitachi) with an operation voltage of 20.0 kV.

Transmission electron microscopy (TEM) and high-resolution TEM (HRTEM) were performed on JEM 2010, JEOL, Japan at an accelerate voltage of 200 kV. The structure analysis was carried out by Bruker D8 Advance X-ray powder diffractometer using Cu Kα radiation (λ = 1.5406 nm) from 5° to 85° at a scan rate of 2° min^{-1}, which operated at voltage 40 kV, current 30 mA. The Brunauer-Emmett-Teller (BET) specific surface area and porosity of obtained samples were detected by Quantachrome, Autosorb-IQ-MP instrument. The composition and chemical states were determined by X-ray photoelectron spectroscopy (XPS) on Thermo VG Scientific ESCALAB 250 spectrometers with Al Kα radiation source (1486 eV). The thermogravimetric analysis (TGA Netzsch, TG209 F3) was operated in air at a heating rate of 5°C min^{-1} from 30°C to 800°C.

1.4. Electrochemical measurements

All the electrochemical measurements were conducted at room temperature (25 °C) using CHI 760E electrochemical workstation (Shanghai Chenhua Co., China). The conventional three-electrode system was employed, including the polished glassy carbon rotating disk electrode (GC, 0.19625 cm^2) loaded with the required catalysts as the working electrode, the saturated calomel electrode (SCE) as the reference electrode, and a Pt wire as the auxiliary electrode, respectively. The electrocatalyst inks were prepared by ultrasonically dispersing 4 mg acquired sample in mixture solution containing 652 μL deionized water, 87 μL 5 wt% Nafion, and 261 μL isopropanol. 10 μL dispersed ink was coated onto the GC electrode with a mass loading ~0.2 mg cm^{-2} for catalyst, then dried in air. All measured potentials were reported versus the standard reversible hydrogen electrode (RHE), and for conversion of the tested potential (vs. SCE):

$$E(RHE) = E(SCE) + 0.059 pH + 0.2415$$

All the OER tests were subsequently tested in 0.1 M KOH solution. The OER linear polarization curves (LSVs) were recorded at scan rate 5 mV s^{-1} ranged between approximately 1.1 and 1.9 V vs. RHE and the data were 80% IR compensated. According to the polarization curves, the Tafel slopes were calculated using the Tafel

equation as follows: η = a + b log (j), where η, a, b and j are the overpotential, Tafel constant, Tafel slope and measured current density, respectively. The overpotential (η) were measured as follows: η (V) = E (vs. RHE)-1.23 V. The electrochemical impedance spectroscopy (EIS) measurements were conducted at 1.60 V (vs. RHE) in the frequency range of 0.01-100000 Hz. Furthermore, the OER durability was evaluated by chronopotentiometric measurements at 10 mA cm^{-2} in 0.1 M KOH electrolyte. Commercial RuO_2 catalyst were also measured for comparison.

All the measurements were carried out in 0.1 M KOH solution for ORR performances. The 0.1 M KOH was bubbled with N_2 or O_2 for at least an hour before cyclic voltammetry (CV) tests, and CV curves were tested at a scan rate of 10 mV s^{-1}. The electrochemical impedance spectroscopy (EIS) was measured at -0.19 V (vs. SCE) with the frequency range from 100000 Hz to 0.01 Hz.

The LSVs were performed at various rotation speeds (i.e., 400, 625, 900, 1225, 1600 and 2025 rpm) due to the diffusion-controlled oxygen reduction reaction (ORR). The kinetic current density and the number of electrons transferred (n) could be calculated from Koutecky-Levich (K-L) plots as the following equation:[2]

$$\frac{1}{J} = \frac{1}{J_L} + \frac{1}{J_K} = \frac{1}{(B\omega^{1/2})} + \frac{1}{J_K} \tag{S1}$$

$$B = 0.62nFC_0D_0{}^{2/3}v^{-1/6} \tag{S2}$$

$$J_K = nFkC_0 \tag{S3}$$

where J, J_k and J_L are the measuring current density, kinetic current density and diffusion limited current density, respectively, while other parameters explain as follows: the reciprocal slope (B), the angular velocity of electrode rotation (ω), the electron transferred number (n), the Faraday constant F (96485 C mol^{-1}), the saturated concentration of O_2 (C_o) in 0.1 M KOH (1.2×10^{-3} mol L^{-1}), the diffusion coefficient of O_2 (D_o) in 0.1 M KOH (1.90×10^{-5} cm^2 s^{-1}), the kinetic viscosity of 0.1 M KOH (υ) (0.01 cm^2 s^{-1}), and the electron transfer rate constant (κ).

RRDE voltammetry were performed at 1600 rpm with a scan speed of 5 mV s^{-1}, and the potential of Pt ring electrode was held at 1.3 V (vs. RHE). The electron transfer number (n) and the hydrogen peroxide yield (H_2O_2%) per oxygen molecule

4

can be calculated by the following equations:

$$n = \frac{4I_D}{I_D + {I_R}/{N}} \tag{S4}$$

$$H_2O_2\% = 200\frac{{I_R}/{N}}{I_D + {I_R}/{N}} \tag{S5}$$

where I_D, I_R and N stand for the disk current, the ring current and ring collection efficiency of RRDE, respectively. In this measurement, N=0.4.

For the Tafel plot, the kinetic current density measured at a rate of 5 mV s^{-1} with a rotating speed from 1600 rpm was calculated from the mass-transport correction of the RDE data by:

$$J_K = \frac{J \times J_L}{(J_L - J)} \tag{S6}$$

The corresponding bifunctional activity parameter was evaluated by ΔE using the following equation:

$$\Delta E = E_{OER,J=10} - E_{1/2} \tag{S7}$$

where $E_{OER,J=10}$ and $E_{1/2}$ are the potential at 10 mA cm^{-2} for OER and half of J_L for ORR, respectively.

The ORR stabilities were examined by chronoamperometry method at constant potential of -0.19 V (vs. SCE) for 10000 s. Furthermore, the poisoning durabilities were performed by the addition of CO and methanol. For comparison, the commercial 20% Pt/C catalysts were operated with the same procedure.

1.5. DFT calculation

First-principles density functional theory (DFT) calculations were carried out using the Vienna Ab Initio Simulation Package (VASP). Geometries were optimized, and the total energies and forces were calculated using a planewave basis set with the projector augmented wave (PAW) method. The generalized gradient approximation (GGA) with the Perdew–Burke–Ernzerhof (PBE) exchange-correlation functional was used, and the planewave cutoff energy was set to 500 eV. All structures were optimized such that the total energy converged to less than 1×10^{-6} eV per atom and the maximum force converged to below -0.01 eV Å^{-1}. Brillouin-zone integrations were carried out using a 5×1×1 Monkhorst–Pack K-point grid. All calculations were

performed using spin restricted method. The dipole correction and Van der Waals correction method was not considered, because they have little influence on the comparison of models' energy in our system.
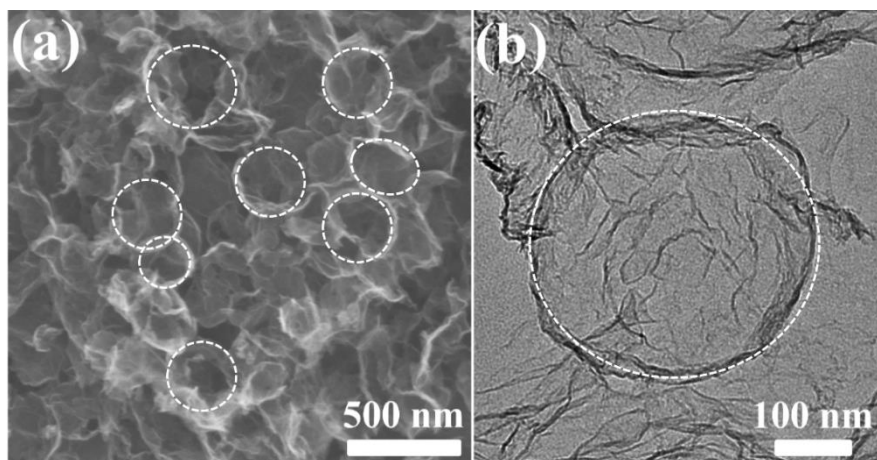
Fig. S1. (a) SEM and (b) TEM images of NGHS. The formed hollow spheres were marked with white circles.
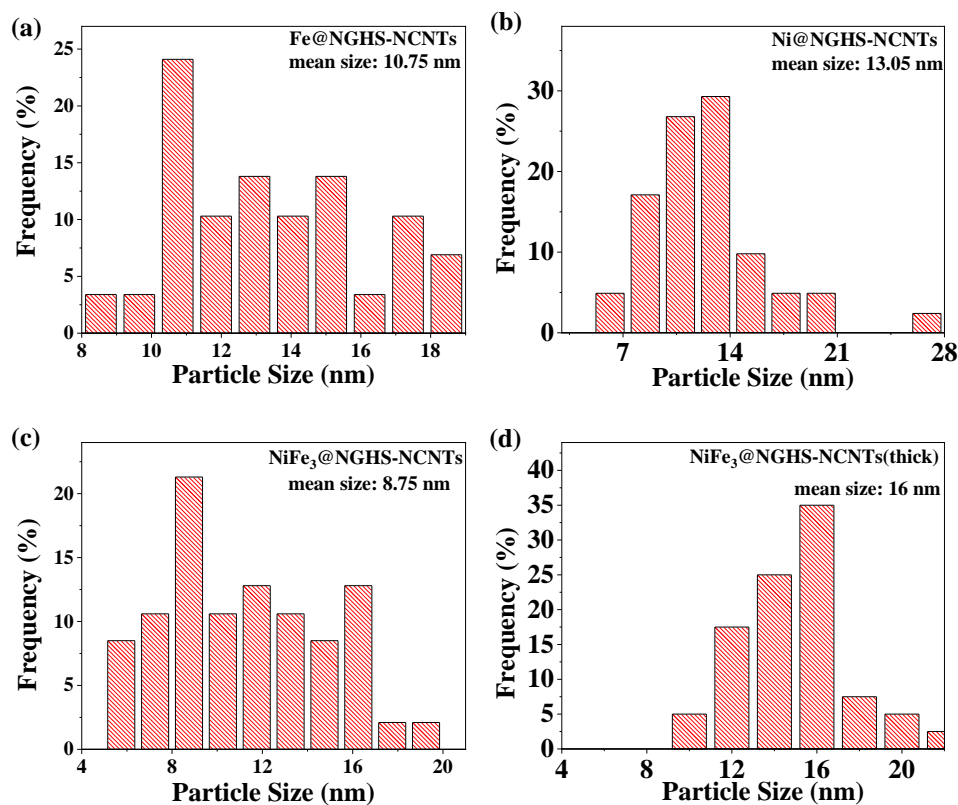
Fig. S2. The particle size distribution diagrams of (a) Fe@NGHS-NCNTs, (b) Ni@NGHS-NCNTs, (c) NiFe$_3$@NGHS-NCNTs, and (d) NiFe$_3$@NGHS-NCNTs(thick).
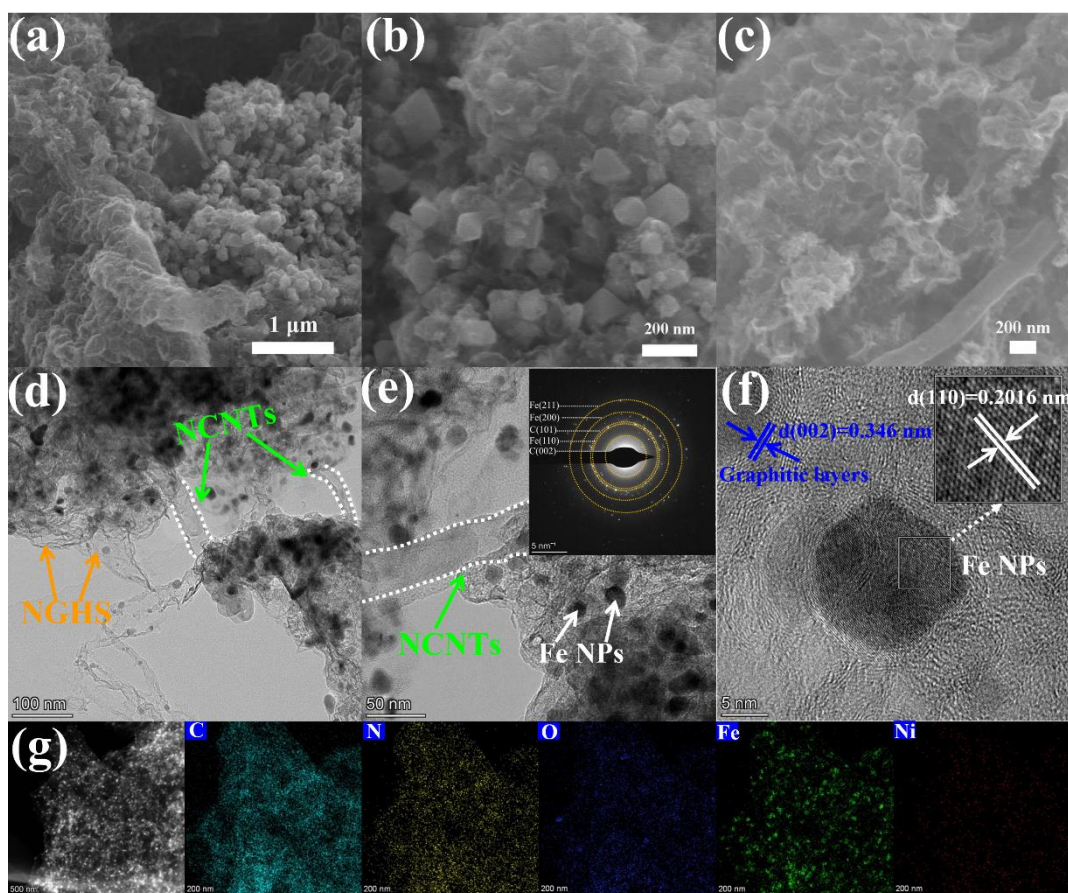
Fig. S3. SEM images of (a, b, c) NiFe$_3$@NGHS-NCNTs(thick). TEM and HRTEM images of (d, e, f) NiFe$_3$@NGHS-NCNTs(thick). (g) EDS elemental mapping images of NiFe$_3$@NGHS-NCNTs(thick). The inset in (e) shows the SAED pattern of NiFe$_3$@NGHS-NCNTs(thick).
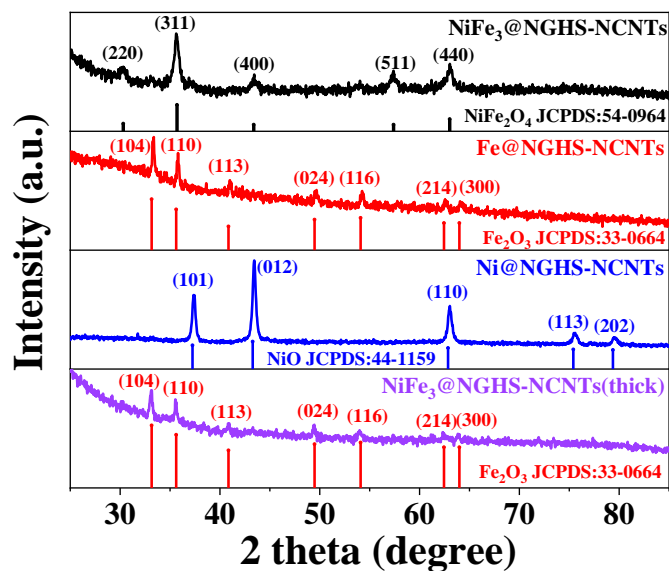
Fig. S4. XRD patterns of NiFe3@NGHS-NCNTs, Fe@NGHS-NCNTs, Ni@NGHS-NCNTs, and NiFe3@NGHS-NCNTs(thick) after calcinated at 800ºC in air.
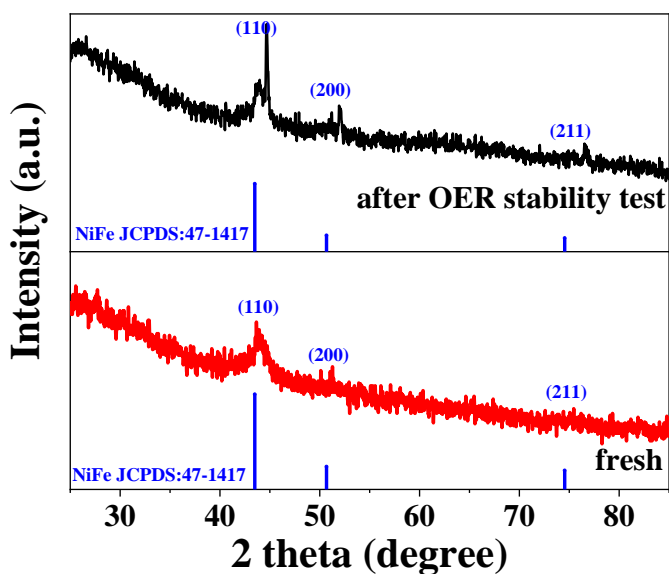
Fig. S5. XRD pattern of NiFe3@NGHS-NCNTs and NiFe3@NGHS-NCNTs after OER stability test.
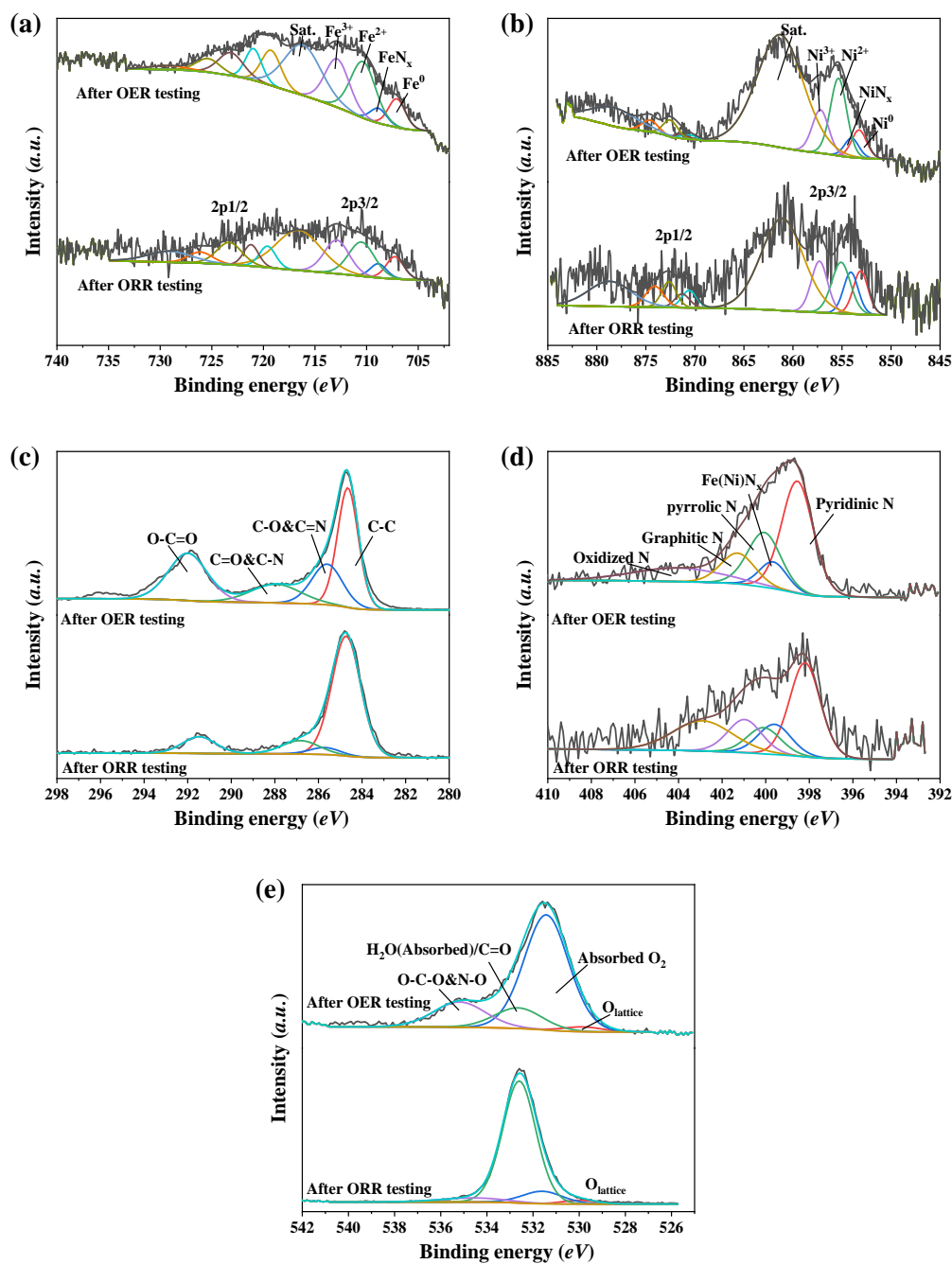
Fig. S6. (a) High-resolution Fe 2p spectra; (b) High-resolution Ni 2p spectra; (c) C 1s, (d) N 1s and (e) O 1s spectra of NiFe$_3$@NGHS-NCNTs after ORR and OER stabilities test.
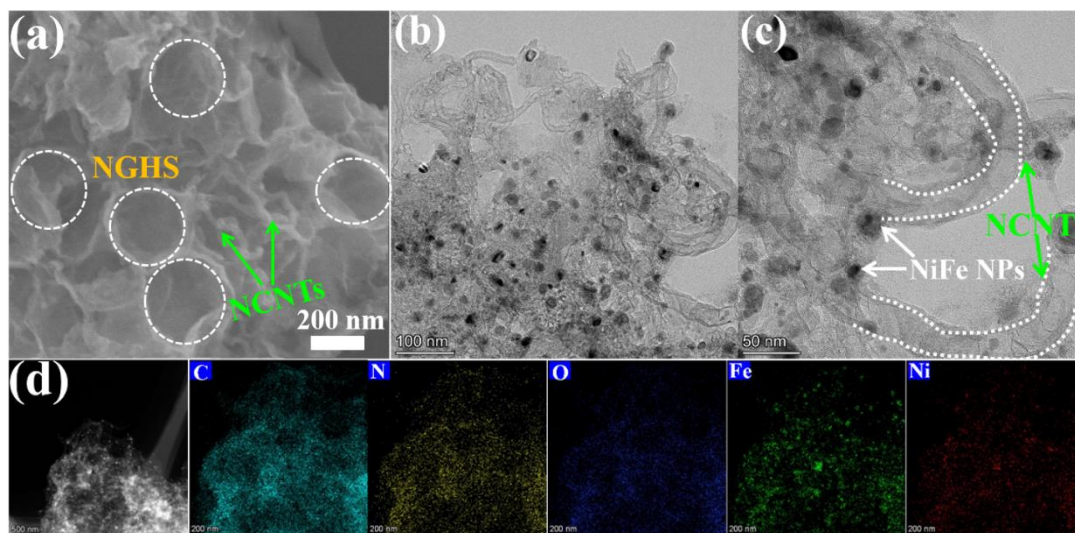
Fig. S7. SEM image (a), TEM images (b, c) and element mapping images (d) of NiFe$_3$@NGHS-NCNTs after OER stability test. The formed hollow spheres were marked with white circles.
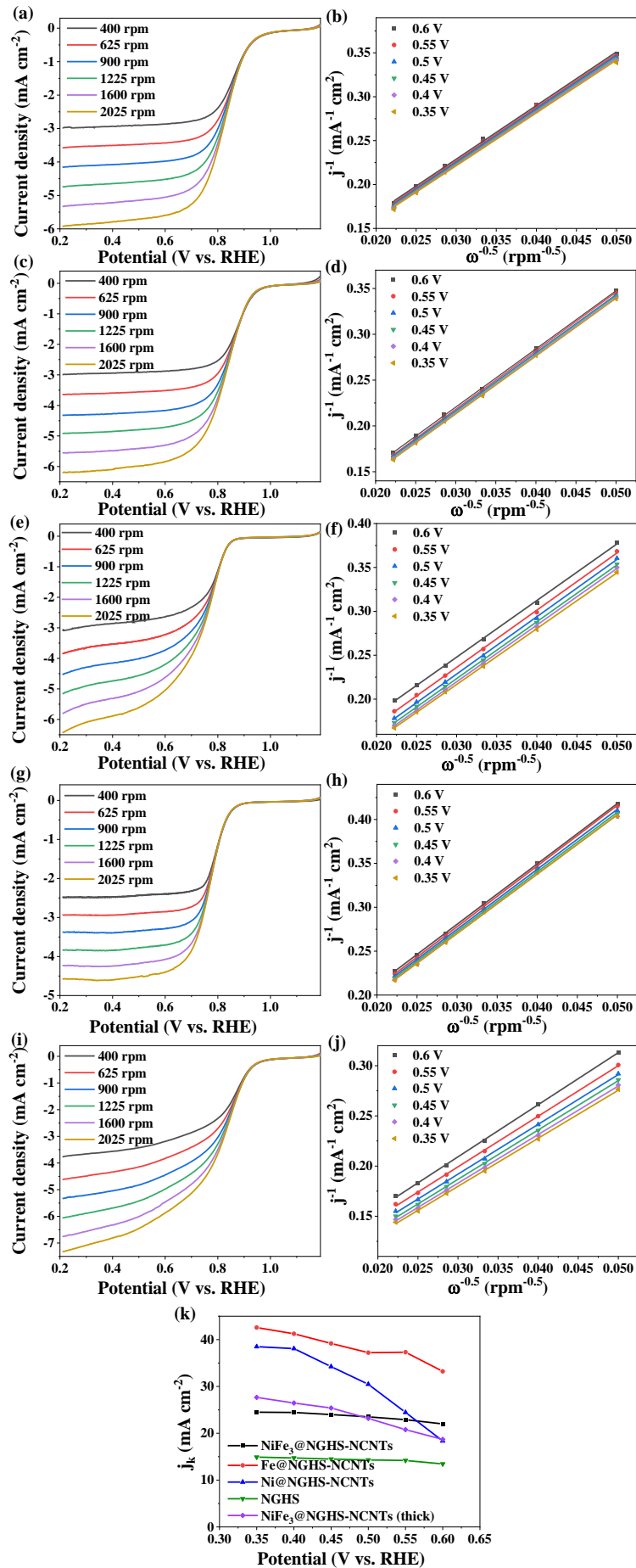
Fig. S8. Rotating disk electrode LSVs of NiFe$_3$@NGHS-NCNTs (a), Fe@NGHS-NCNTs (c), Ni@NGHS-NCNTs (e), NGHS (g) and NiFe$_3$@NGHS-NCNTs(thick) (i) in O$_2$-saturated 0.1 M KOH at different rotation rates (scan rate: 5 mV s^{-1}); Koutecky-Levich plots of ORR obtained at NiFe$_3$@NGHS-NCNTs (b), Fe@NGHS-NCNTs (d), Ni@NGHS-NCNTs (f), NGHS (h) and NiFe$_3$@NGHS-NCNTs (thick) (i) based on the data extracted from (a, c, e, g, i); (k) kinetic current densities.
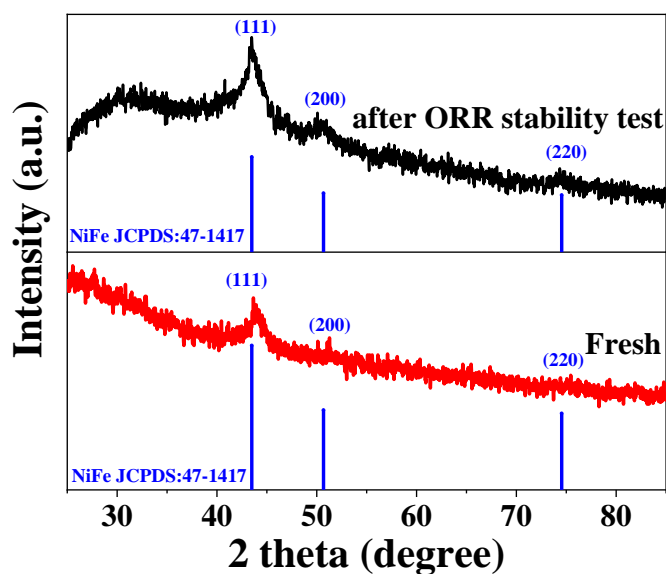
Fig. S9. XRD patterns of NiFe$_3$@NGHS-NCNTs before and after ORR stability test.
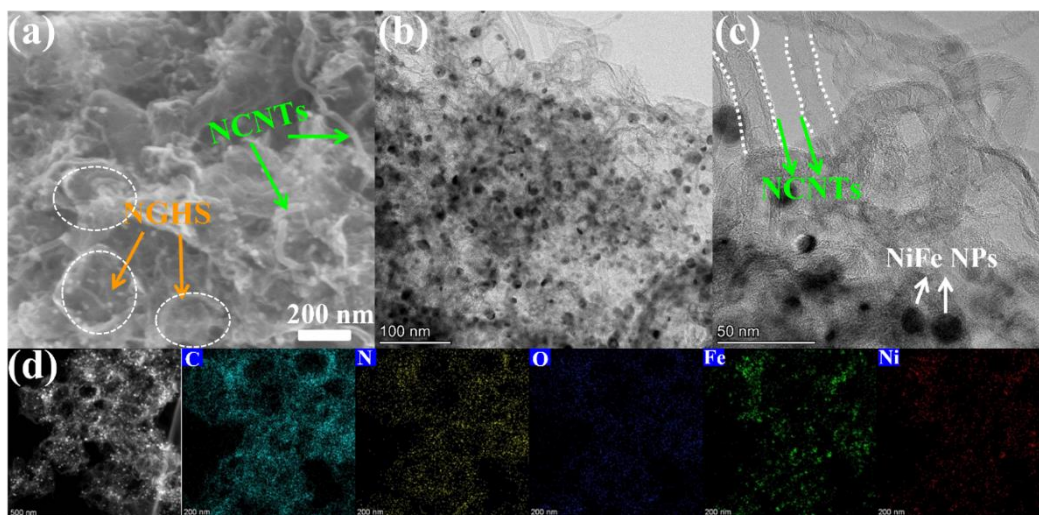
Fig. S10. SEM image (a), TEM images (b, c), and element mapping images (d) of NiFe$_3$@NGHS-NCNTs after ORR stability test. The formed hollow spheres were marked with white circles.

12
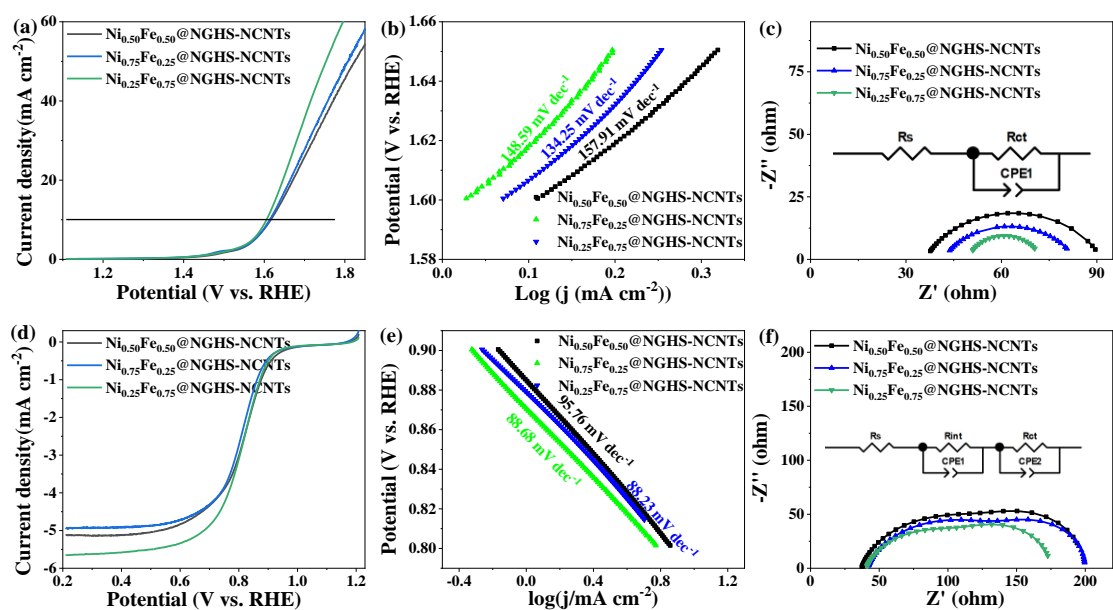
Fig. S11. OER performances: (a) OER polarization LSV curves, (b) Tafel curves, (c) EIS Nyquist plots. ORR performances: (d) ORR polarization LSV curves, (e) Tafel curves, (f) EIS Nyquist plots of NiFe@NGHS-NCNTs prepared in different intermetallic molar ratios, maintaining other parameters such as total metal loading of 1 mmol and calcination temperature of 800 °C.
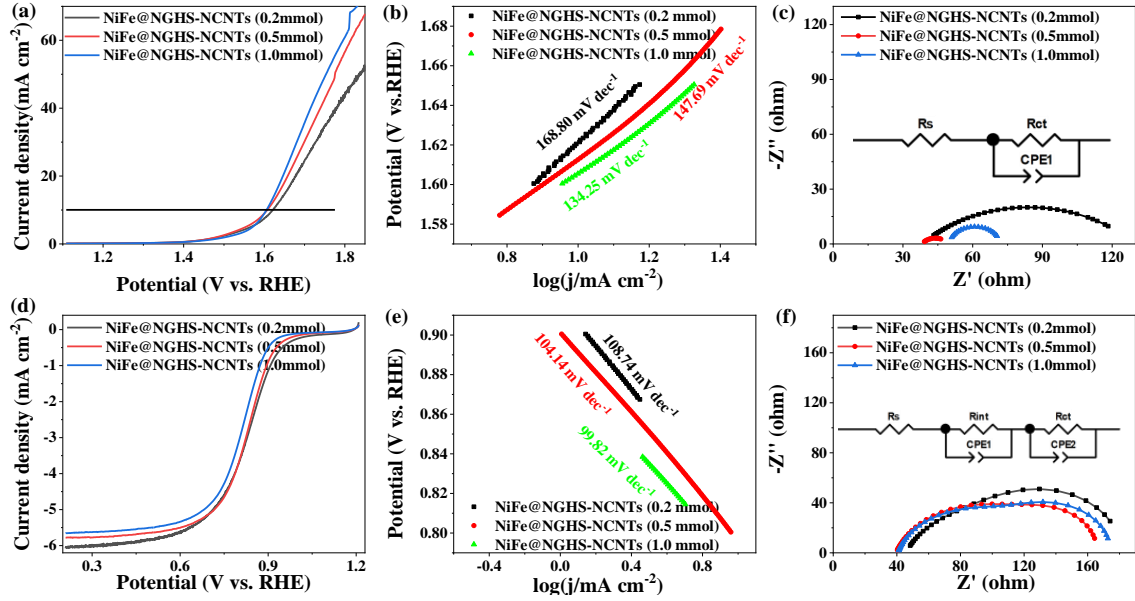
Fig. S12. OER performances: (a) OER polarization LSV curves, (b) Tafel curves, (c) EIS Nyquist plots. ORR performances: (d) ORR polarization LSV curves, (e) Tafel curves, (f) EIS Nyquist plots of NiFe@NGHS-NCNTs prepared at different alloy loadings, maintaining other parameters such as intermetallic molar ratio of 1:3 (Ni : Fe) and calcination temperature of 800 °C.
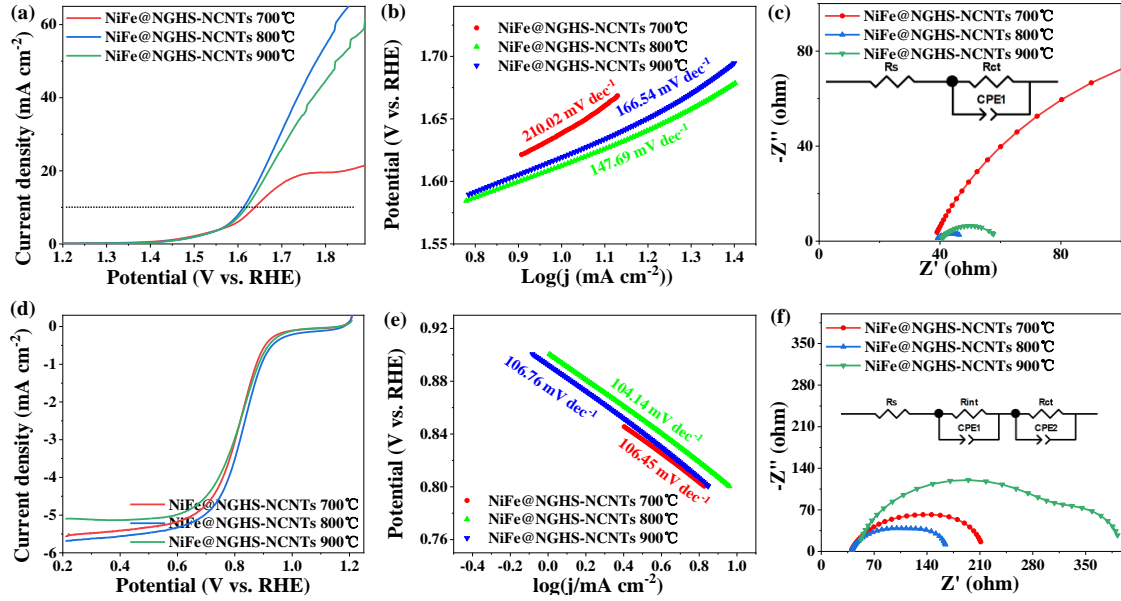
Fig. S13. OER performances: (a) OER polarization LSV curves, (b) Tafel curves, (c) EIS Nyquist plots. ORR performances: (d) ORR polarization LSV curves, (e) Tafel curves, (f) EIS Nyquist plots of NiFe@NGHS-NCNTs prepared at different calcination temperatures, maintaining other parameters such as intermetallic molar ratio of 1:3 (Ni:Fe) and alloy loading of 0.5 mmol.

Table S1. Summary of element contents in the as-prepared samples determined by XPS.

Catalysts	C (at%)	N (at%)	Fe (at%)	Ni (at%)	O (at%)
NiFe$_3$@NGHS-NCNTs	85.87	10.09	0.38	0.21	3.45
Fe@NGHS-NCNTs	81.89	9.2	0.64	-	8.28
Ni@NGHS-NCNTs	82.16	9.84	-	0.64	7.36
NGHS	88.81	8.87	-	-	2.32
NiFe$_3$@NGHS-NCNTs(thick)	80.94	9.97	1.10	0.01	7.98

Table S2. Nitrogen species in the as-prepared samples determined by XPS using N 1s.

	Pyridinic-N		Fe(Ni)N$_x$		Pyrrolic-N		Graphitic-N		Oxidized-N	
	Binding energy (eV)	Content (%)	Binding energy (eV)	Content (%)	Binding energy (eV)	Content (%)	Binding energy (eV)	Content (%)	Binding energy (eV)	Content (%)
NiFe$_3$@NGHS-NCNTs	398.65	47.58	399.57	9.46	400.1	3.11	401.05	30.33	403.01	9.51
Fe@NGHS-NCNTs	398.45	46.04	399.57	7.70	400.1	13.0	401.0	20.34	402.92	12.91
Ni@NGHS-NCNTs	398.63	47.19	399.41	4.81	400.0	17.27	401.01	23.80	403.06	6.93
NGHS	398.25	41.71	-	-	399.85	10.59	400.93	36.59	403.03	11.10
NiFe$_3$@NGHS-NCNTs(thick)	398.4	43.06	399.61	4.28	400.11	27.87	401.31	13.98	404.11	10.81

Table S3. Electrocatalytic properties of NiFe$_3$@NGHS-NCNTs and recently reported transition metal-based catalysts for ORR and OER.

Catalysts	ORR		OER	ΔE (V vs. RHE)	Reference
	E$_{onset}$ (V vs. RHE)	E$_{1/2}$ (V vs. RHE)	E$_{J=10}$ (V vs. RHE)		
NiFe$_3$@NGHS-NCNTs	0.97	0.823	1.613	0.791	This work
FeNi$_3$N/NG	0.88	0.79	1.64	0.85	[3]
NiFe/N-CNT	-	0.75	1.52	0.77	[4]
Ni$_3$Fe/N-C sheets	0.90	0.78	1.6	0.82	[5]
Ni$_3$FeN/NRGO	1.38	0.75	1.63	0.88	[6]
Ni$_3$FeN microspheres	-	0.78	1.585	0.805	[7]
FeNi-NC	0.98	0.83	1.61	0.78	[8]
NiFe-ND/FeCo-NC	0.93	0.85	1.66	0.81	[9]
NiFe@N-CFs	0.94	0.82	1.53	0.71	[10]
nNiFe LDH/3D MPC	-	0.862	1.57	0.708	[11]
Fe$_{1.2}$Co@NC/NCNTs	0.842	0.821	1.585	0.765	[12]
FeCo$_2$O$_4$/hollow graphene(HG)	0.92	0.82	1.65	0.83	[13]
CoFe$_2$O$_4$/CNTs	0.904	0.75	1.65	0.9	[14]
FeCo@NC-750	0.94	0.8	1.49	0.69	[15]
CoFe/N-C	1.03	0.821	1.665	0.844	[16]
CoFe@NCNTs	0.95	0.84	1.68	0.84	[17]
Ni$_x$Co$_{(3-x)}$O$_4$/NH$_2$-CNTs	0.948	0.851	1.615	0.764	[18]
NiCo/PFC	0.86	0.79	1.63	0.84	[19]
NiCo$_2$O$_4$	0.93	0.78	1.62	0.84	[20]
Fe$_x$Ni$_y$N@C/NC	0.98	0.87	1.53	0.67	[21]

Table S4. Summary of the impedance fitting data for catalysts during ORR process.

Catalysts	Resistance(Ω)			CPE1(mF)		CPE2(mF)	
	R_s	R_{int}	R_{ct}	CPE1-T	CPE1-P	CPE2-T	CPE2-P
NiFe$_3$@NGHS-NCNTs	39.58	93.24	33.84	2.02×10^{-3}	0.7993	0.0248	1.0940
Fe@NGHS-NCNTs	47.44	77.88	54.13	3.12×10^{-3}	0.7671	0.0161	1.0580
Ni@NGHS-NCNTs	48.19	54.81	182.40	1.62×10^{-3}	0.8059	0.0035	0.9929
NGHS	41.18	41.13	102.20	1.67×10^{-3}	0.8853	0.0186	0.9954
NiFe$_3$@NGHS-NCNTs(thick)	49.26	76.22	76.43	2.56×10^{-3}	0.8317	0.0114	0.9642
Pt/C	39.88	23.23	86.43	2.23×10^{-3}	0.8392	0.0038	0.9702

R_s represents solution resistance in the electrolyte, R_{int} represents solid-electrolyte interface resistance, R_{ct} represents charge-transfer resistance and CPE represents constant phase elements.

Table S5. Summary of the impedance fitting data for catalysts during OER process.

Catalysts	Resistance(Ω)		CPE(mF)	
	R_s	R_{ct}	CPE-T	CPE-P
NiFe$_3$@NGHS-NCNTs	38.18	11.44	2.19×10^{-4}	0.6406
Fe@NGHS-NCNTs	38.44	43.40	2.19×10^{-3}	0.7166
Ni@NGHS-NCNTs	38.19	653.20	9.90×10^{-6}	0.9431
NGHS	35.35	117.20	1.45×10^{-4}	0.6563
NiFe$_3$@NGHS-NCNTs(thick)	40.18	242.20	1.48×10^{-4}	0.6165
RuO$_2$	37.26	31.75	2.77×10^{-4}	0.7945

Table S6. Bader charge distribution of the catalysts.

NiFe₃@NC		Fe@NC		Ni@NC		NC		NiFe₃@NC	
Atoms	**Bader charge**	**Atoms**	**Bader charge**	**Atoms**	**Bader charge**	**Atoms**	**Bader charge**	**Atoms**	**Bader charge**
C1	0.055	C1	-0.105	C1	-0.106	C1	-0.103	C1	-0.078
C2	-0.022	C2	0.002	C2	0.001	C2	0.099	C2	0.062
C3	0.208	C3	0.167	C3	0.168	C3	0.173	C3	-0.085
C4	-0.052	C4	-0.028	C4	-0.033	C4	0.013	C4	0.058
C5	0.161	C5	0.040	C5	0.043	C5	0.059	C5	-0.021
C6	-0.182	C6	-0.052	C6	-0.059	C6	-0.063	C6	-0.049
C7	0.205	C7	0.004	C7	0.004	C7	0.173	C7	-0.097
C8	-0.222	C8	-0.024	C8	-0.028	C8	-0.195	C8	0.003
C9	0.068	C9	0.065	C9	0.066	C9	0.054	C9	-0.074
C10	0.279	C10	0.216	C10	0.284	C10	0.163	C10	0.292
C11	-0.106	C11	-0.106	C11	-0.106	C11	-0.107	C11	0.026
C12	0.454	C12	0.443	C12	0.442	C12	0.448	C12	0.421
C13	-0.106	C13	-0.106	C13	-0.105	C13	-0.107	C13	-0.075
C14	-0.051	C14	0.069	C14	0.063	C14	0.073	C14	0.036
C15	0.036	C15	0.011	C15	0.014	C15	-0.093	C15	-0.061
C16	0.070	C16	0.070	C16	0.071	C16	0.091	C16	-0.055
C17	0.039	C17	-0.042	C17	-0.041	C17	-0.278	C17	0.053
C18	0.023	C18	0.094	C18	0.056	C18	0.030	C18	-0.085
C19	0.203	C19	0.179	C19	0.187	C19	0.237	C19	0.033

C20	-0.139	C20	-0.225	C20	-0.229	C20	-0.256	C20	-0.087
C21	0.205	C21	0.236	C21	0.171	C21	0.320	C21	0.130
C22	-0.241	C22	-0.207	C22	-0.213	C22	-0.224	C22	0.048
C23	0.282	C23	0.146	C23	0.290	C23	0.163	C23	0.290
C24	0.056	C24	0.051	C24	0.053	C24	0.054	C24	-0.076
C25	-0.011	C25	0.094	C25	0.095	C25	0.092	C25	0.091
C26	0.025	C26	-0.094	C26	-0.091	C26	-0.102	C26	0.035
C27	0.147	C27	0.145	C27	0.146	C27	0.092	C27	-0.055
C28	0.441	C28	0.451	C28	0.509	C28	0.693	C28	0.509
C29	0.332	C29	0.436	C29	0.449	C29	0.552	C29	0.270
C30	0.225	C30	0.214	C30	0.215	C30	0.257	C30	0.144
C31	-0.161	C31	-0.229	C31	-0.225	C31	-0.256	C31	-0.203
C32	0.201	C32	0.303	C32	0.165	C32	0.320	C32	0.164
C33	-0.219	C33	-0.050	C33	-0.151	C33	-0.195	C33	-0.025
C34	0.194	C34	0.024	C34	0.120	C34	0.173	C34	-0.104
C35	-0.052	C35	-0.040	C35	-0.041	C35	-0.016	C35	0.007
C36	0.034	C36	-0.066	C36	-0.066	C36	-0.090	C36	0.045
C37	-0.055	C37	-0.049	C37	-0.051	C37	-0.069	C37	0.068
C38	0.503	C38	0.510	C38	0.525	C38	0.583	C38	0.449
C39	-0.196	C39	-0.183	C39	-0.194	C39	-0.023	C39	0.051
C40	0.346	C40	0.375	C40	0.432	C40	0.552	C40	0.304
C41	0.037	C41	0.111	C41	0.111	C41	0.030	C41	-0.069
C42	0.207	C42	0.049	C42	0.052	C42	0.237	C42	0.149
C43	-0.172	C43	0.071	C43	0.066	C43	-0.063	C43	-0.060
C44	0.165	C44	-0.086	C44	-0.081	C44	0.059	C44	-0.021

C45	0.052	C45	0.225	C45	0.220	C45	0.071	C45	-0.015
C46	0.419	C46	0.315	C46	0.322	C46	0.419	C46	0.296
C47	0.211	C47	0.211	C47	0.210	C47	0.104	C47	-0.041
C48	-0.162	C48	-0.064	C48	-0.065	C48	-0.069	C48	0.072
C49	0.498	C49	0.495	C49	0.517	C49	0.583	C49	0.475
C50	0.129	C50	0.129	C50	0.129	C50	0.092	C50	-0.058
C51	0.437	C51	0.443	C51	0.467	C51	0.693	C51	0.397
C52	-0.078	C52	0.060	C52	0.058	C52	0.091	C52	-0.060
C53	0.020	C53	-0.054	C53	-0.052	C53	-0.278	C53	-0.077
C54	-0.032	C54	-0.009	C54	-0.013	C54	0.013	C54	0.053
C55	0.208	C55	0.167	C55	0.169	C55	0.173	C55	-0.077
C56	-0.212	C56	-0.178	C56	-0.179	C56	-0.173	C56	0.060
C57	0.063	C57	0.078	C57	0.080	C57	0.071	C57	0.591
C58	0.053	C58	0.079	C58	0.079	C58	0.071	C58	-0.014
C59	0.404	C59	0.398	C59	0.402	C59	0.419	C59	0.299
C60	-0.034	C60	-0.020	C60	-0.024	C60	-0.016	C60	0.012
C61	0.032	C61	-0.064	C61	-0.062	C61	-0.090	C61	0.053
C62	0.092	C62	0.094	C62	0.095	C62	0.092	C62	0.089
C63	0.041	C63	-0.086	C63	-0.085	C63	-0.102	C63	0.019
C64	-0.065	C64	0.067	C64	0.062	C64	0.073	C64	0.044
C65	0.184	C65	-0.088	C65	-0.086	C65	-0.093	C65	-0.050
C66	-0.196	C66	0.100	C66	0.099	C66	0.099	C66	-0.029
N1	-1.141	N1	-1.137	N1	-1.144	N1	-1.148	N1	-1.139
N2	-1.193	N2	-1.200	N2	-1.207	N2	-1.183	N2	-1.147
N3	-1.168	N3	-1.141	N3	-1.171	N3	-1.014	N3	-1.151

N4	-1.203	N4	-1.201	N4	-1.204	N4	-1.188	N4	-1.199
N5	-1.248	N5	-1.173	N5	-1.176	N5	-1.254	N5	-1.127
Fe1	0.112	Fe1	0.024	Ni1	0.012			Fe1	0.003
Fe2	0.108	Fe2	0.044	Ni2	0.009			Fe2	0.630
Fe3	0.658	Fe3	0.585	Ni3	0.554			Fe3	0.099
Ni1	-0.203	Fe4	0.019	Ni4	0.005			Fe4	0.094
								Fe5	0.000
								Fe6	0.027
								Fe7	0.146
								Fe8	0.348
								Fe9	0.147
								Fe10	0.020
								Fe11	0.355
								Fe12	0.125
								Ni1	-0.047
								Ni2	-0.240
								Ni3	-0.310
								Ni4	-0.029

Table S7. Comparison of liquid and solid Zn-air performances of the NiFe$_3$@NGHS-NCNTs catalyst with recently reported advanced catalysts.

References	Catalysts	liquid Zn-air battery		solid Zn-air battery	
		power density (mW cm^{-2})	specific capacity (mA h g^{-1})	open-circuit voltage (V)	power density (mW cm^{-2})
This work	NiFe$_3$@NGHS-NCNTs	126.54	808.7 (200 mA cm^{-2})	1.44	102.82
[3]	FeNi$_3$N/NG	115.3	785.2 (10 mA cm^{-2})	1.463	-
[10]	NiFe@N-CFs	102	719 (5 mA cm^{-2})	-	-
[22]	NPC/FeCo@NCNT	151.3	810 (200 mA cm^{-2})	1.45	65.0
[23]	NGM-Co	152	750 (20 mA cm^{-2})	1.439	-
[24]	CoN$_4$/NG	-	730 (100 mA cm^{-2})	-	28
[25]	CoS$_x$/CoNC-800	103	734.2 (40 mA cm^{-2})	1.34	-
[26]	o-CC-H$_2$	91.4	707 (20 mA cm^{-2})	1.258	-
[27]	Fe-Co$_4$N@NC	105	806 (5 mA cm^{-2})	1.34	72
[28]	(Zn,Co)/NSC	150	-	1.56	15
[29]	IOSHs-NSC	133	768 (10 mA cm^{-2})	1.408	60
[30]	NGCNT/FeCo	89.3	653.2 (100 mA cm^{-2})	1.249	97.8
[31]	Co$_9$S$_8$/MnS-USNC	146.77	-	1.34	79

References

1. Q. Shen, Z. Jiang, X. Tian, H. Zhu and Z.-J. Jiang, *J. Alloy. Compd.*, 2021, **884**, 161073.

2. I. S. Amiinu, Z. Pu, X. Liu, K. A. Owusu, H. G. R. Monestel, F. O. Boakye, H. Zhang and S. Mu, *Adv. Funct. Mater.*, 2017, **27**, 1702300.

3. L. Liu, F. Yan, K. Li, C. Zhu, Y. Xie, X. Zhang and Y. Chen, *J. Mater. Chem. A*, 2019, **7**, 1083-1091.

4. H. Lei, Z. Wang, F. Yang, X. Huang, J. Liu, Y. Liang, J. Xie, M. S. Javed, X. Lu, S. Tan and W. Mai, *Nano Energy*, 2020, **68**, 104293.

5. G. Fu, Z. Cui, Y. Chen, Y. Li, Y. Tang and J. B. Goodenough, *Adv. Energy Mater.*, 2017, **7**, 1601172.

6. Y. Fan, S. Ida, A. Staykov, T. Akbay, H. Hagiwara, J. Matsuda, K. Kaneko and T. Ishihara, *Small*, 2017, **13**, 1700099.

7. G. Fu, Z. Cui, Y. Chen, L. Xu, Y. Tang and J. B. Goodenough, *Nano Energy*, 2017, **39**, 77-85.

8. L. Yang, X. Zeng, D. Wang and D. Cao, *Energy Storage Mater.*, 2018, **12**, 277-283.

9. Y. Wang, G. Zhang, M. Ma, Y. Ma, J. Huang, C. Chen, Y. Zhang, X. Sun and Z. Yan, *Sci. China Mater.*, 2020, **63**, 1182-1195.

10. Y. Niu, X. Teng, S. Gong and Z. Chen, *J. Mater. Chem. A*, 2020, **8**, 13725-13734.

11. W. Wang, Y. Liu, J. Li, J. Luo, L. Fu and S. Chen, *J. Mater. Chem. A*, 2018, **6**, 14299-14306.

12. S. Li, W. Chen, H. Pan, Y. Cao, Z. Jiang, X. Tian, X. Hao, T. Maiyalagan and Z.-J. Jiang, *ACS Sustain. Chem. Eng.*, 2019, **7**, 8530-8541.

13. W. Yan, Z. Yang, W. Bian and R. Yang, *Carbon*, 2015, **92**, 74-83.

14. X. Zhang, H. Xu, X. Li, Y. Li, T. Yang and Y. Liang, *ACS Catalysis*, 2016, **6**, 580-588.

15. P. Cai, S. Ci, E. Zhang, P. Shao, C. Cao and Z. Wen, *Electrochim. Acta*, 2016, **220**, 354-362.

16. T. An, X. Ge, N. N. Tham, A. Sumboja, Z. Liu and Y. Zong, *ACS Sustain. Chem. Eng.*, 2018, **6**, 7743-7751.

17. P. Cai, Y. Hong, S. Ci and Z. Wen, *Nanoscale*, 2016, **8**, 20048-20055.

18. B. Chen, Z. Jiang, J. Huang, B. Deng, L. Zhou, Z.-J. Jiang and M. Liu, *J. Mater. Chem. A*, 2018, **6**, 9517-9527.

19. G. Fu, Y. Chen, Z. Cui, Y. Li, W. Zhou, S. Xin, Y. Tang and J. B. Goodenough, *Nano Lett.*, 2016, **16**, 6516-6522.

20. M. Prabu, K. Ketpang and S. Shanmugam, *Nanoscale*, 2014, **6**, 3173-3181.

21. M. Wu, G. Zhang, Y. Hu, J. Wang, T. Sun, T. Regier, J. Qiao and S. Sun, *Carbon Energy*, 2020, **3**, 176-187.

22. X. Hao, Z. Jiang, B. Zhang, X. Tian, C. Song, L. Wang, T. Maiyalagan, X. Hao and Z. J. Jiang, *Adv. Sci.*, 2021, **8**, 2004572.

23. C. Tang, B. Wang, H. F. Wang and Q. Zhang, *Adv. Mater.*, 2017, **29**, 1703185.

24. L. Yang, L. Shi, D. Wang, Y. Lv and D. Cao, *Nano Energy*, 2018, **50**, 691-698.

25. Q. Lu, J. Yu, X. Zou, K. Liao, P. Tan, W. Zhou, M. Ni and Z. Shao, *Adv. Funct. Mater.*, 2019, **29**, 1904481.

26. H.-F. Wang, C. Tang, B. Wang, B.-Q. Li, X. Cui and Q. Zhang, *Energy Storage Mater.*, 2018, **15**, 124-130.

27. Q. Xu, H. Jiang, Y. Li, D. Liang, Y. Hu and C. Li, *Appl. Catal. B-Environ.*, 2019, **256**, 117893.

28. C. Li, M. Wu and R. Liu, *Appl. Catal., B*, 2019, **244**, 150-158.

29. K. Tang, C. Yuan, Y. Xiong, H. Hu and M. Wu, *Appl. Catal. B-Environ.*, 2020, **260**, 118209.

30. C.-Y. Su, H. Cheng, W. Li, Z.-Q. Liu, N. Li, Z. Hou, F.-Q. Bai, H.-X. Zhang and T.-Y. Ma, *Adv. Energy Mater.*, 2017, **7**, 1602420.

31. J. Li, W. Li, H. Mi, Y. Li, L. Deng, Q. Zhang, C. He and X. Ren, *J. Mater. Chem. A*, 2021, **9**, 22635-22642.